Optimal catalyst thickness in titanium dioxide fixed film reactors: mathematical modelling and experimental validation.

Massimiliano Vezzoli[a,b,*], Troy Farrell[b], Adrian Baker[b], Steven Psaltis[b], Wayde N. Martens[b], John M. Bell[b]

[a] *Chemistry Faculty, University of Bath, Bath, UK*
[b] *Science and Engineering Faculty, Queensland University of Technology, Brisbane, Australia*

Abstract

The use of immobilised TiO_2 for the purification of polluted water streams introduces the necessity to evaluate the effect of mechanisms such as the transport of pollutants from the bulk of the liquid to the catalyst surface and the transport phenomena inside the porous film. Experimental results of the effects of film thickness on the observed reaction rate for both liquid-side and support-side illumination are here compared with the predictions of a one-dimensional mathematical model of the porous photocatalytic slab. Good agreement was observed between the experimentally obtained photodegradation of phenol and its by-products, and the corresponding model predictions. The results have confirmed that an optimal catalyst thickness exists and, for the films employed here, is 5 µm.Furthermore, the modelling results have highlighted the fact that porosity, together with the intrinsic reaction kinetics are the parameters controlling the photocatalytic activity

*corresponding author: m.vezzoli@bath.ac.uk

of the film. The former by influencing transport phenomena and light absorption characteristics, the latter by naturally dictating the rate of reaction.

Keywords: photocatalysis, titanium dioxide, intrinsic kinetics, optimal thickness, mass transport, porosity

1. Introduction

While fixed-film titanium dioxide photocatalysis has been suggested as a very promising technology for water purification [1, 2], many issues have hindered its application on a commercial scale [3, 4]. The applicability of this technology on a large scale highly depends on the effective utilisation of the photocatalytic surface and the incident radiation flux obtained from either natural or artificial sources to destroy the organic pollutants present in the stream. Intimate interaction between the catalyst, pollutants and radiation is necessary for efficient photocatalysis, and this makes the optimization and design of photocatalytic reactors in general a very complex task. The thickness of the catalyst plays an important role in the performance of the reactor. Together with factors such as porosity, total surface area and light absorption coefficient it influences the final pollutant conversion and the photocatalytic efficiency of the system [5, 6, 7]. In slurry reactors investigations of the catalyst concentration [8, 5, 9, 10, 11] have shown that the amount of titania per unit volume of solution directly influences the radiation distribution and, hence, the photocatalytic activity inside the slurry. As a result, its optimisation is key if the highest possible photon efficiency and pollutant conversion are the goal [9, 10, 11, 12, 13]. In a similar fashion, varying the thickness of the titania layer in a fixed film reactor will change both the avail-

able catalyst surface and the amount of light absorbed, ultimately affecting the observed rate of reaction and the final pollutant conversion [14, 15, 12]. In a reactor configuration where the catalyst is illuminated from the solution-side, here defined liquid-side (LS) illumination following Ray [16], it can be expected that once the film thickness has reached a value that allows for almost complete absorption of the incoming photons, any further thickness increase will provide no advantage since the "lower" layers of the film will receive little or no radiation and therefore will not be able to contribute to the reaction. A simplified representation of the photon and pollutant fluxes for the LS illumination is depicted in Fig. 1A. If the light is introduced from the support-side (SS) (i.e. through the glass-titania interface), the photons and the pollutant fluxes have opposite directions and a single optimal thickness value has been proposed to exist rather than a plateau [14]. A clear explanation of this phenomenon was given by Chen et al. [14] considering the generation of hydroxyl radicals and the diffusion of pollutants in porous media. If the film is very thin, the generated charges and hydroxyl radicals are created in an area where the pollutants are abundant. When the film thickness is increased, up to a certain critical value, the reaction rate will increase due to the increased light absorption and consequent higher production of hydroxyl radicals. However, for films thicker than this critical value, the observed pollutant conversion will decrease since the radicals will be generated in an area were the reactants will be scarce due to the diffusion limitations. The thicker the film, the greater the separation between the areas with the maximum charge concentration (glass-titania interface) and maximum pollutant concentration (liquid-titania interface), with the actual

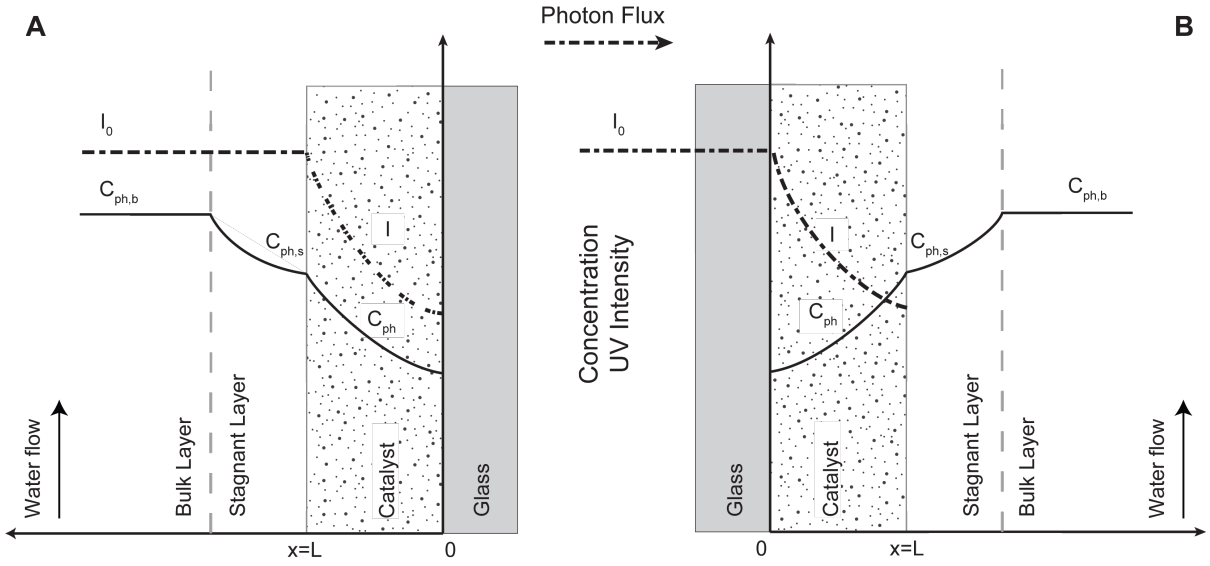

Figure 1: A - Schematic of the LS illumination system where pollutant and photon flux come from the same direction. B - Schematic of the SS illumination where pollutant and photon flux come from opposite directions.

value for optimal thickness determined by the light absorption and internal diffusion characteristics of the film. A simplified schematic representation of radiation and concentration profiles for the SS illumination is shown in Fig. 1B. While the LS configuration is probably the most commonly used in lab-scale reactors, the SS illumination configuration holds particular interest for commercial applications since in many practical situations the turbidity of the water and the thickness of the fluid layer above the catalyst could greatly reduce the UV radiation available for the excitation of the titanium oxide substrate. The optimization of the catalyst thickness is fundamental for the successful migration of this technology from the laboratory to the real world. Knowing its effects on the final photocatalytic activity will help in

the design of more efficient reactors and will facilitate the application of this technology on a large scale. In this paper we present an accurate and validated mathematical model of the photocatalytic activity of porous titania substrates. This will provide a modelling tool that can be used to identify key parameters for the process as well as test various "what if" scenarios aimed at facilitating device optimisation. In this study, the experimental results obtained from the investigation of the effect of film thickness on phenol degradation for both LS and SS configurations are compared with the predictions of the mathematical model for the description of the photocatalytic activity of a porous film. The model developed in this work highlights the influence of pollutant diffusion and advection in the film, accounts for the film optical properties through the absorption coefficient and uses values of the intervening parameters that have been experimentally derived or are well-established in the literature. The Beer-Lambert law adopted for light modeling is a significant but effective simplification. If effects due to much higher radiation intensities [5, 17], internal scattering [5, 17] or just a higher complexity due to the geometry of the reactor are introduced, an effort for the implementation of more complex models might be necessary [5, 18, 12, 19, 20, 21].

The governing equations are solved numerically using the control-volume method [22] and the degradation curves obtained are directly compared to the experimental results. While this type of study has been proposed by other groups [14, 15, 23] in their work, some major simplifications and assumptions were made. The simplification of a concentration profile controlled by an exponential law was adopted by Chen et al. [14]. The dimensionless anal-

ysis proposed by Camera-Roda and Santarelli [15] was limited to the porous photocatalytic film and the influence of external factors was not considered. All studies used a simplified linear rate equation where only the concentration of the target pollutant was related to the rate of reaction [14, 23, 15]. The model proposed here, on the other hand, employs a competitive site Langmuir-Hinshelwood rate equation to describe the photocatalytic activity of the titania film, and calculates the degradation rate of phenol and its by-products modelled as a single group of reaction intermediates. The kinetic parameters used here are obtained from a previous study [24]. Importantly, the model developed here uses a dimensionless coefficient in order to be able to adopt true kinetic parameters obtained from experimental set-ups that operates in comparable conditions of illumination and UV intensity/spectral range (those should be the most common in photocatalytic applications). This achievement is key for the practical applications of model presented. Moreover, the model proposed here provides a complete description of the experimental set-up, the effects of external mass transfer on the reactants concentration at the liquid-solid boundary are accounted for, as described in Vezzoli *et al.*[24], and have a direct effect on the model equations that describe the porous medium where diffusion, light absorption and photocatalytic reaction take place. Finally, the investigation of light and pollutant transport phenomena clearly shows the importance of the physical characteristics of the porous film (i.e. light absorption constant, kinetic parameters, porosity and morphology) that control the photocatalytic reaction. The model developed could ultimately help in the prediction of the effects that a change to those physical parameters, obtained in the material synthesis phase, will have on

the photocatalytic activity of the film.

2. Experimental

2.1. Experimental setup, photocatalytic experiments and sample analysis

The operation and design of the photocatalytic reactor used in this work is thoroughly described elsewhere [24]. The method and mathematical model used to obtain true kinetic parameters for phenol photocatalytic degradation were also presented in the previous publication. In this work, the same flat plate reactor was used for the investigation of the effect of film thickness over the observed rate of phenol degradation. The reactor flow channel has a total length of 540 mm and a maximum width of 98 mm; the area where the photocatalytic plates are placed and illuminated is 98 mm wide, 220mm long and the channel depth is constant at 1 mm. In this work a new top flange was used, allowing the use of 3.2 mm thick borosilicate glass plates (Schott Borofloat 33). The borosilicate glass plate serves as both window and titania support for the SS illumination experiments. Fig. 2 shows the reactor with the two different top flanges used to create LS and SS configuration. The two flanges were machined so that the channel geometry and flow conditions are the same in both experiments; the difference in the window thickness, 8 mm quartz window for LS illumination experiments and 3.2 mm borosilicate glass window for SS experiments, was accounted for by measuring the difference in average UV irradiance reaching the catalyst surface. The transparency of the quartz window for the UVA radiation used allowed an average irradiance of 70.7 W m^{-2} for the LS experiments while the slightly higher absorption due to the borosilicate glass and the positioning of the titania film produced

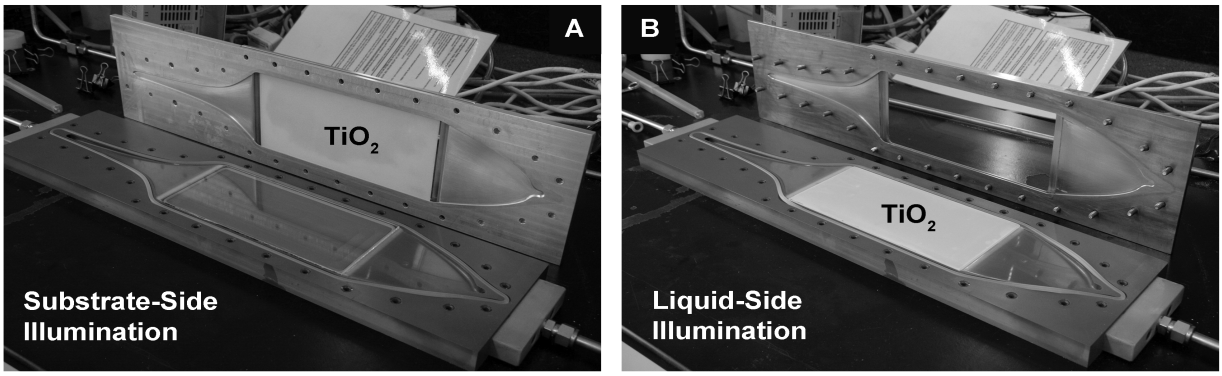

Figure 2: A - Reactor in the SS illumination configuration, the bottom recess is occupied by a clean glass plate and the internal surface of the window is coated in titania. B - Reactor in the LS illumination configuration, the bottom recess is occupied by a photocatalytic plate and the window is an 8 mm thick quartz plate.

an average UVA irradiance of 65.3 W m^{-2} for the SS experiments (i.e. the irradiance reported is the value measured at evaluated at x=L for LS and at x=0 for SS). The UV irradiance reaching the catalyst surface was accurately measured by employing potassium ferrioxalate actinometry and following the method described by Montalti [25] and Murov [26]. The values reported only consider the portion of light that can be usefully employed in titanium dioxide photocatalysis (i.e. λ<388 nm).

The UV radiation was provided by seven NEC FL15BL 15W UVA lamps with an emission spectrum between 310 and 410 nm wavelength (peak output at 365 nm), positioned perpendicularly to the flow direction and held in position by a specially designed support [24]. A constant water flow rate of 5 l min^{-1} was maintained within the reactor during all experiments with the use of a gear pump (Micropump GC-M35 with Ismatec Drive ISM506). Stainless steel tubing ($3/8^{th}$ inch) was used for the connections with a reser-

voir consisting of a glass vessel with cooling jacket of 3 litres total volume. A Julabo EF35 cooling unit was connected to the jacket in order to keep the reacting solution at 25 °C for the duration of the experiments; a magnetic stirrer was used to ensure that the solution in the reservoir was well mixed. Instrument grade air (BOC) for conduction band electrons scavenging was supplied at 3 l min^{-1} through a bubbler situated in the reservoir. The water sampling was performed from the reservoir at regular intervals (15 minutes) buy using a peristaltic pump (Gilson Manipulus 3) and a fraction collector (Gilson FC-204). Analytical work was carried out using an Agilent HPLC equipped with a Agilent XDB C8 column for phenol detection and a Shimadzu TOC analyzer. The photocatalytic experiments were performed by first circulating 1.6 litres of aqueous solution containing phenol at a concentration of 20 ppm for 20 minutes in the absence of UV light. Photocatalytic activity was subsequently initiated by removing the window cover. At that time, a total reaction time of 2 or 3 hours was allowed for the LS or SS illumination respectively. Further details on the experimental setup and the methods used can be found in a previous publication [24].

2.2. Photocatalytic plates preparation

For both LS and SS illumination, borosilicate glass plates (Schott Borofloat 33) were used for supporting the photocatalyst. The area coated with titanium dioxide was maintained constant (215.6 cm^2) by using a mask during the spraying process. Before the spraying procedure, the glass plates were soaked in a piranha solution bath (70% sulphuric acid, 30% hydrogen peroxide) overnight and rinsed with MillQ water. A methanol solution of titanium dioxide Degussa P25 (about 0.035 g ml^{-1}) was sonicated for 30 minutes and

Table 1: Average thickness and measurements 95% confidence interval for LS plates and SS plates.

Plate	Thickness (µm)	95% C.I. (µm)	Plate	Thickness (µm)	95% C.I. (µm)
LS 1	0.52	0.14	SS 1	0.86	0.12
LS 2	1.21	0.33	SS 2	1.37	0.16
LS 3	2.24	0.29	SS 3	1.84	0.19
LS 4	4.77	0.98	SS 4	2.49	0.17
LS 5	7.01	0.68	SS 5	4.57	0.49
			SS 6	7.58	0.53
			SS 7	9.44	0.65
			SS 8	13.33	1.48

then sprayed on the glass support. The coated glass plates were calcined for 2h at 450 °C at a heating rate of 4.5 °C min^{-1}. Two sets of photocatalytic plates were prepared for the investigation of the effect of film thickness on the reaction rate for both LS and SS illumination. The average thicknesses of the titanium dioxide films were estimated via SEM imaging and are reported, together with a 95% confidence interval, in Table 1. The average thickness obtained on each plate could be controlled quite easily by spraying a defined amount of solution; the required thickness and uniformity were achieved by spraying multiple titanium dioxide layers on the plates, with adequate time between successive coats to allow the titania layer to dry on the plate, thus avoiding excessive deposition on local areas. The light absorption coefficient, $\alpha = 0.6\ \mu m^{-1}$, was calculated from spectrometric measurements performed with a UV-Vis spectrometer equipped with an integrating sphere on films of

a range of thicknesses.

3. Theoretical modeling

3.1. Model development

Following our previous work [24], where the photocatalytic degradation of phenol was simplified in a two-step reaction in which the variety of phenol degradation by-products were represented by one single generic reaction intermediate, namely

$$C_6H_6OH \longrightarrow Intermediate \longrightarrow CO_2 \tag{1}$$

the same concept was applied to the modelling of the photocatalytic reaction taking place inside the titanium dioxide porous slab. Consequently, the reaction rate term R_i (mol m^{-3} s^{-1}) for each single reactant, namely phenol ($_{ph}$), intermediate ($_I$) and carbon dioxide ($_{cd}$), can be represented by the following competitive site Langmuir-Hinshelwood (L-H) type equations,

$$R_{ph} = -\frac{k_{ph}K_{ph}C_{ph}}{1 + K_{ph}C_{ph} + K_IC_I}E^n, \tag{2}$$

$$R_I = \frac{k_{ph}K_{ph}C_{ph} - k_IK_IC_I}{1 + K_{ph}C_{ph} + K_IC_I}E^n \tag{3}$$

and

$$R_{cd} = \frac{k_IK_IC_I}{1 + K_{ph}C_{ph} + K_IC_I}E^n \tag{4}$$

Here k_{ph}(mol m^{-1}s^{-1}W^{-1}), K_{ph} (m^{3}mol^{-1}) and C$_{ph}$(mol m^{-3}) are the reaction rate constant, the adsorption equilibrium constant and the concentration of phenol, respectively. Furthermore, k_I, K_I and C$_I$ are the reaction rate

constant, the adsorption equilibrium constant and the concentration of the intermediates, respectively, E (W m^{-2}) is the UV irradiance and n is a constant that represents the relationship between light and reaction rate. Unless high-pressure lamps or concentrated light are used in the reactor, the rate of reaction is generally found to be first order with the UV irradiance [27, 17]. Adopting this approach, the degradation of phenol and its by-products over time can be easily followed by analysing only the phenol concentration and the total organic carbon contained in the solution using simple HPLC and TOC techniques as noted in the previous section. While its the authors' opinion that the choice of this system of rate equations delivers a grater flexibility and a broader applicability to the model due to the way it can deal with the presence of intermediate products, it is also true that it can be simply substituted with any other specific rate equation that the user might deem useful.

The photocatalytic titania film is modelled here as a one-dimensional porous film of thickness L attached to a glass support on one side (x=*0*), and being in contact with the fluid solution on the other, (x=L), as presented in Fig. 1A and 1B. Noting Eqns. (2) to (4) the conservation of solution phase species is given by [28],

$$\varepsilon_{sol}\frac{\partial C_{ph}}{\partial t} = \varepsilon_{sol}D_{e,ph}\frac{\partial^2 C_{ph}}{\partial x^2} - \frac{\partial}{\partial x}(C_{ph}v^0) - A\frac{k_{ph}K_{ph}C_{ph}}{1+K_{ph}C_{ph}+K_IC_I}E^n, \qquad (5)$$

$$\varepsilon_{sol}\frac{\partial C_I}{\partial t} = \varepsilon_{sol}D_{e,I}\frac{\partial^2 C_I}{\partial x^2} - \frac{\partial}{\partial x}(C_Iv^0) + A\,\frac{k_{ph}K_{ph}C_{ph}-k_IK_IC_I}{1+K_{ph}C_{ph}+K_IC_I}E^n, \qquad (6)$$

$$\varepsilon_{sol}\frac{\partial C_{cd}}{\partial t} = \varepsilon_{sol}D_{e,cd}\frac{\partial^2 C_{cd}}{\partial x^2} - \frac{\partial}{\partial x}(C_{cd}v^0) + A\,\frac{k_IK_IC_I}{1+K_{ph}C_{ph}+K_IC_I}E^n, \qquad (7)$$

and

$$\varepsilon_{sol}\frac{\partial C_{H_2O}}{\partial t} = \varepsilon_{sol}D_{e,H_2O}\frac{\partial^2 C_{H_2O}}{\partial x^2} - \frac{\partial}{\partial x}(C_{H_2O}v^0). \tag{8}$$

Here ε_{sol} is the volume fraction of the porous film that is occupied by the solution (composed of water, phenol, reaction intermediates and carbon dioxide),C_i (mol m^{-3}) is the concentration of species i per unit volume of solution phase and v^0 (m s^{-1}) is the bulk average velocity of the fluid in the film. In Eqns. (5) to (8), $D_{e,i}$ (m^2 s^{-1}) is the effective diffusivity of species i in the film and is given by [29, 7]

$$D_{e,i} = D_i^{\infty}\frac{\varepsilon_{sol}}{\tau} \tag{9}$$

where D_i^{∞} is the diffusion coefficient of species i, ε_{sol} the porosity of the catalyst and τ the tortuosity. A value of $\sqrt{3}$ was assigned to the tortuosity as suggested by Froment [30] and Dijkstra [7] while the porosity of the film was evaluated from FESEM images and estimated to be 0.57. The parameter A in Eqns. (5) to (8) accounts for the fact that in our previous work [24] the regression analysis that was performed to obtain the kinetic parameters $(k_{ph}, k_I, K_I, K_{ph})$ did not explicitly account for the porosity of the film, the thickness of the film or for the fraction of incident light actually absorbed by the film. Our porous film model, however, does explicitly account for these and it also accounts for both LS and SS illumination conditions. Thus, there exist a discrepancy between the simple model that was applied previously to obtain our kinetic parameters and the current, more sophisticated porous film model. In order to account for these differences the following dimensionless

multiplier A was included in all reaction rate terms in Eqns. (5) to (8),

$$A = \frac{(BET)\rho S(1-\varepsilon_{sol})}{S}\frac{1-\exp^{-\alpha L_{max}}}{1-\exp^{-\alpha L_{exp}}} = (BET)\rho(1-\varepsilon_{sol})\frac{1-\exp^{-\alpha L_{max}}}{1-\exp^{-\alpha L_{exp}}} \tag{10}$$

Here BET is the catalyst surface area per unit mass, typically 55 m^2g^{-1} for Degussa P25 used in this work [31],ρ is the density of the material (4.31 g cm^{-3}) [31], S is the geometrical surface of the photocatalytic plate (0.02156 m^2), L_{exp} (m) is the thickness of the film used for the experimental evaluation of the kinetic parameters (4.9 µm), and L_{max} is the film thickness at which 98% of the incident light is absorbed by the film (6 μm). When Beer-Lambert (Eq. 14) is used in combination with the material UV light absorption constant measured ($\alpha = 0.6$ μm^{-1}) , it can be calculated that a film thickness of 6 µm absorbs 98% of the incident light, making any further increase in thickness of little or no impact at all. This value was considered a reasonable threshold to be used as the maximum thickness of an activated photocatalytic film. The first part of Eq. (10) represents the ratio of the total active surface area of a photocatalytic film (here taken to be characterised by the BET area) to the geometric surface area of the film. The second part of the expression, again calculated using Beer-Lambert and the light absorption coefficient, is the ratio of the maximum UV light absorption possible in a porous titanium dioxide film of this type and the light absorption actually achieved by the film used for the experimental determination of the four kinetic parameters (4.9 µm thick). It must be stressed that by introducing the parameter A described by Eq. (10) in all rate terms in Eqns. (5) to (8), the kinetic parameters calculated on any film using the method previously reported [24] can now be adopted in the model proposed here to

estimate the effects of catalyst thickness on the observed reaction rate. For instance, if a very thick film was used in the experiments for the evaluation of the material kinetic activity, parameter A will account for the fact that only the surface area created by the upper 6 μm of catalyst is actually actively participating in the reaction, neglecting the surface area developed by the bottom catalyst thickness that is not reached by any light. On the other hand, if a very thin film was used, the porous film model can account for the fact that the kinetic parameters are misleadingly low because obtained with a film that had limited active surface area and limited light absorption.

Conservation of volume within the liquid phase dictates that,

$$\overline{V}C_{ph} + \overline{V}C_I + \overline{V}_{cd}C_{cd} + \overline{V}_{H_2O}C_{H_2O} = 1, \tag{11}$$

where $\overline{V_i}$ (m^3mol^{-1}) is the partial molar volume of the species i. This equation allows us to remove C_{H_2O} as an unknown in our model system, given the concentrations C_{ph}, C_I and C_{cd}. Differentiating Eq. (11) with respect to time and substituting Eq. (5) to (8) we may obtain an equation for the velocity, v^0. In doing this we note that is reasonable to assume that phenol and its by-products will have a similar diffusion coefficient ($D_{ph} = 0.89 \times 10^{-9} m^2 s^{-1}$)[32] and that the diffusion coefficient for carbon dioxide ($1.91 \times 10^{-9} m^2 s^{-1}$)[33] is approximately equal to that of phenol. While this could seem a bit far-fetched, the assumption can be considered quite reasonable once the very low rate of cd formation and the fact that it does not compete in the rate equations are taken into consideration. Given this we assume that the effective diffusion coefficients of all of the species present in solution are equal, that is $D_{e,ph} = D_{e,I} = D_{e,cd} = D_{e,H_2O} = D_e$. Combined with the aforementioned manipulations of Eq. (12) this yields the following equation for

v^0;

$$\frac{\partial v^0}{\partial x} = \overline{V_{ph}} A R_{ph} + \overline{V_I} A R_I + \overline{V_{cd}} A R_{cd}. \tag{12}$$

Eq. (12) states that only the oxidative reaction contributes to the development of a velocity field inside the porous catalyst. In a system where the main flow runs on top and parallel to a microscopically porous slab (Fig. 1A), we do not expect the external flow field velocity to significantly influence the velocity field inside the porous material. (Must be noticed that, in the mass balance of Eq. 7, the correct valued was used for the diffusion of carbon dioxide).

As commonly adopted in literature [14, 15, 23, 34], the attenuation of UV light irradiance inside the titania film will be treated according to the Beer-Lambert law [35], namely,

$$E = E_0 \exp^{-\alpha l}, \tag{13}$$

where E (W m^{-2}) is the UV irradiance at the specific film depth, E_0(W m^{-2}) is the incoming irradiance, α (m^{-1}) is the absorption coefficient for the material at the considered wavelength and l (m) is the length of the path travelled by the light inside the absorbing material.

Due to the characteristics of the catalyst, two major assumptions were made; the first regarding the light incidence angle and the second regarding the light absorption characteristics of the films. Since most of the photons reaching the titania surface comes from the lamp directly above the point considered, the assumption of a beam perpendicular to the surface is considered reasonable. Furthermore, properly accounting for the scattering effects inside a porous titanium dioxide film is extremely difficult and can be considered

matter for a separate publication. If a system with much higher radiation intensities, or affected by much higher scattering level are adopted [5, 17] or, if a system characterised by a much more complex light path due to the reactor geometry and the catalyst support is adopted [18, 12, 19, 21], more complex models, like the one here referenced here should be considered [5, 18, 12, 19, 20, 21]. Although polychromatic radiation was used, the model was developed by assuming monochromatic radiation and by adopting the absorption coefficient calculated at 365 nm (peak wavelength in the broad lamp emission spectrum).

Eq. (13) will be modified to account for the differences between the SS illumination, where the maximum irradiance is at the glass/titania interface, and the LS illumination, where the maximum value is at the titania-liquid interface. According to the coordinate system adopted in Fig. 1A and 1B, where the origin is placed at the interface between glass support and titanium dioxide, the length of the path travelled by the light inside the film, can be defined differently depending on the light propagating direction. For the SS illumination, the distance travelled by the radiation inside the porous medium, l, will correspond to the coordinate value, x, and Beer-Lambert can be written as,

$$E = E_0 \exp^{-\alpha x}, \tag{14}$$

$$E = E_0 \exp^{-\alpha(L-x)}. \tag{15}$$

At this point, all the fundamental equations have been defined and the boundary conditions must be established. At the interface between glass and titanium dioxide, where no exchange of molecules is possible, a zero-flux

condition can be imposed for all species so that,

$$\varepsilon_{sol} D_e \frac{\partial C_i}{\partial x}\bigg|_{x=0}. \tag{16}$$

In addition, a no-penetration condition at this boundary gives,

$$v^0 = 0. \tag{17}$$

On the opposite side of the catalyst film, where the catalyst is in contact with the flow of water and pollutants running through the reactor, the model that describes the underlying photocatalytic process described so far must be coupled to a stagnant film model that describes the flux of pollutants across a thin layer of quiescent liquid that forms an interface between the porous film and the bulk fluid. Such thin film models are common at interfaces where the bulk flow is parallel to a solid surface [28, 36]. By doing this, the oxidation of molecules in the porous film will directly affect the observed rate of pollutant degradation in the bulk of the fluid, where the experimental concentration measurements are taken. Thus, at the x=L boundary we set

$$\varepsilon_{sol} D_e \frac{\partial C_i}{\partial x}\bigg|_{x=L} - (C_i v^0)\big|_{x=L} = k_{m,i}(C_{i,b} - C_i|_{x=L}), \tag{18}$$

where $k_{m,i}$ (m s^{-1}) is the mass transfer coefficient of phenol and phenol by-products (assumed here to be equal) and carbon dioxide, $C_{i,b}$ (mol m^{-3}) are the concentrations of phenol, intermediates and carbon dioxide in the bulk of the fluid and $C_i|_{x=L}$ (mol m^{-3}) are these same concentrations at the x=L boundary. The bulk concentrations, $C_{i,b}$, are assumed to be linearly proportional to the concentrations $C_i|_{x=L}$, such that at x=L we may write,

$$\frac{dC_{i,b}}{dt} = k_{m,i} a (C_{i,b} - C_i|_{x=L}) \frac{V_r}{V_{tot}}. \tag{19}$$

Here a (m^{-1}) is the ratio of the geometric surface area of the catalyst film to the volume of the reactor, V_r (m^3), and V_{tot} (m^3) is the total volume of solution used for the reaction. The initial condition imposed on the model assume that at $t = 0$ the film is in equilibrium with the bulk of the solution and the concentration of phenol, C_{ph}, is the same everywhere, with a specific value of 20 ppm, corresponding to approximately 1252 mmol m^{-3} of carbon. Furthermore, the initial concentration of by-products is assumed to be 0. Thus, at $t=0$,

$$C_{ph} = C_{ph,b} = 1252\,(mmol\,m^{-3}), \tag{20}$$

$$C_I = C_{I,b} = C_{cd} = C_{cd,b} = 0\,(mmol\,m^{-3}), \tag{21}$$

and

$$v^0 = 0\,(m\,s^{-1}). \tag{22}$$

At this point it might be worth highlighting the importance of external mass transfer in any kind of kinetic modelling applied to fixed film photocatalysis. Neglecting the mass transfer across the boundary layer at the liquid-titania interface is a very common mistake and can lead to gross miscalculation in the rate of reactions and the obtained pollutant conversions. For example, it was calculated that in the conditions of UV light and initial substrate concentration adopted in this work, with $Re \simeq 1900$, the concentration in the stagnant layer could be safely considered 15-20% lower than that in the bulk of the fluid at the beginning of the experiment, with the difference increasing of roughly another 5-10% as the reaction progresses. As a consequence, it is paramount that the external mass transfer effect is accounted for if a reliable

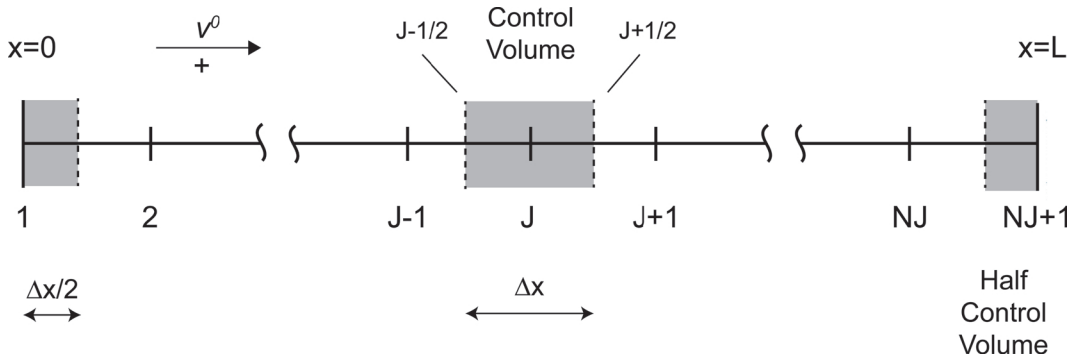

Figure 3: Schematic of the control-volume grid adopted.

prediction is needed. Summarising, in this section the governing model equations have been established (Eqns. 5,6,7 and12) and the attenuation of light inside the film defined by Eq. (14) or (15) depending on the illumination (i.e. SS or LS). The boundary conditions, to be applied for all three species, have been defined by Eqns. (16) to (19) with the initial conditions given by Eqns. (20) to (22).

3.2. Solution technique and model parameters

The governing equations presented in Section 3.1 were solved numerically by adopting the control volume technique described by Patankar [22]. Following this method, the catalyst film was discretised in a 1-D mesh (Fig. 3) with the control nodes equally distributed on the length of the mesh and positioned at the centre of the discrete volumes (Δx); the only exception being points 1 and NJ+1 at the domain extremities where half control volumes (Δx/2) were used. Since the experimental setup provided a very uniform illumination and a very low conversion per pass ($<$0.2%) the use of a 1-D model was considered an appropriate simplification. The governing equa-

tions were discretised with respect to space. Time stepping was performed by the ODE15s solver [37] used in the Matlab code written for the numerical solution of the model. In the discretisation of the diffusion terms, the grid-point value of the variables C_{ph}, C_I and C_{cd} was assumed to prevail throughout the control volume (yielding a so called "linear piecewise profile " for these variables [22]). An up-winding scheme [22] was applied to the convective terms in which the value of the concentration of species i at the control volume faces are taken to be equal to the value of the variable at the "upwind" grid-point. In order for the model predictions to be compared with the results of the experiments described in Section 2.1, the simulations covered a time-span of 2 hours for the LS configuration and 3 hours for the SS illumination configuration, both with time-steps of 100 seconds. Shorter time-steps were tested and no significant change in the predictions was observed. After appropriate testing, a grid of 100 points was selected as our standard grid. The list of physical and kinetic parameters used in the model is reported in Table 2. It is important to note that no "free" parameters have been used in this work and all the values reported in Table 2 have been experimentally established or obtained from appropriate literature.

4. Results and Discussion

A comparison between model predictions and experimental results for the total phenol conversion is presented in Fig. 4 for LS illumination and in Fig. 5 for SS illumination. In both cases, a good agreement between predicted and measured values can be observed. In Fig. 4 the experimental results

Table 2: Model parameters.

Parameter	Value	Parameter	Value
$\varepsilon_{\mathrm{sol}}$	0.57	$\mathrm{V_{tot}}$	1.6 (litres)
$D_{e,ph}$	2.929×10^{-10} ($\mathrm{m^2 s^{-1}}$)	$\mathrm{V_r}$	0.02156 (litres)
$D_{e,cd}$	6.286×10^{-10} ($\mathrm{m^2 s^{-1}}$)	$\overline{V_{\mathrm{ph}}}$, $\overline{V_{\mathrm{I}}}$	86.17 ($\mathrm{cm^3\ mol^{-1}}$)[38]
k_m	$8.576\times10^{-7}\ \mathrm{Re}^{0.65}$	$\overline{V_{\mathrm{cd}}}$	39 ($\mathrm{cm^3\ mol^{-1}}$) [39]
a	1000 ($\mathrm{m^{-1}}$)	k_{ph}	0.5226 ± 0.028 ($\mathrm{mmol\ m^{-1}\ s^{-1}\ W^{-1}}$)
E_0 (LS)	70.7 ($\mathrm{W\ m^{-2}}$)	k_I	0.120 ± 0.0088 ($\mathrm{mmol\ m^{-1}\ s^{-1}\ W^{-1}}$)
E_0 (SS)	65.3 ($\mathrm{W\ m^{-2}}$)	K_{ph}	$8.5\times10^{-4} \pm 1\times10^{-4}$ ($\mathrm{m^3\ mmol^{-1}}$)
n	1[24]	K_I	$2.2\times10^{-3} \pm 3\times10^{-4}$ ($\mathrm{m^3\ mmol^{-1}}$)
α	0.6 ($\mu\mathrm{m^{-1}}$)	Re	1890

for LS illumination are reported with 95% confidence intervals for both the average film thickness and the final phenol conversion. It can be observed that the model predictions give a good match to the experimental results; within 5% difference across the range of thicknesses trialled.

In Fig. 4, the experimental and modelled change in phenol photocatalytic conversion obtained for different film thicknesses is in good agreement with what explained in the Introduction. An increase in film thickness coincides with an increase in photocatalytic conversion up to 5 µm thickness where, due to the light absorption characteristics of the film, the large majority of the photons (96%) are absorbed by the catalyst. As film thickness increase beyond 5 µm a significant increase in the photocatalytic activity of the film is not observed, nor predicted, since very little light will penetrate the layers of the film beyond the 5 µm value. This behaviour, where light absorption

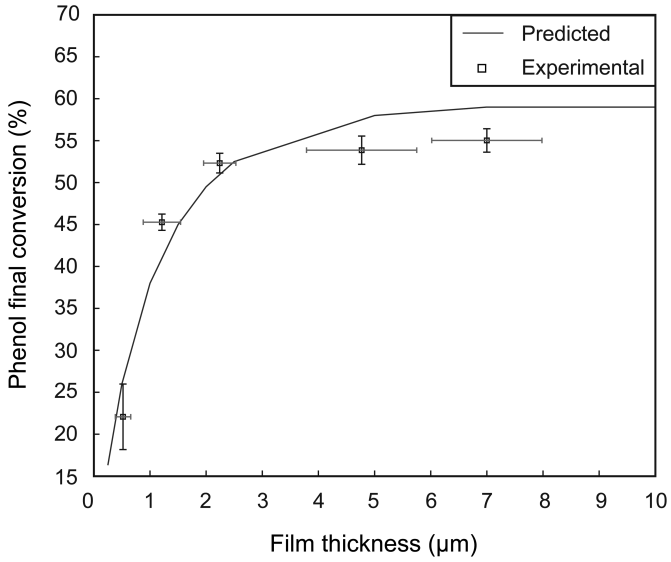

Figure 4: LS configuration. Comparison between predicted and experimental final phenol conversions. Reaction time 2 hours, E_0= 70.7 W m^{-2}. Experimental results are reported with 95% confidence intervals for both average thickness and final phenol conversion values.

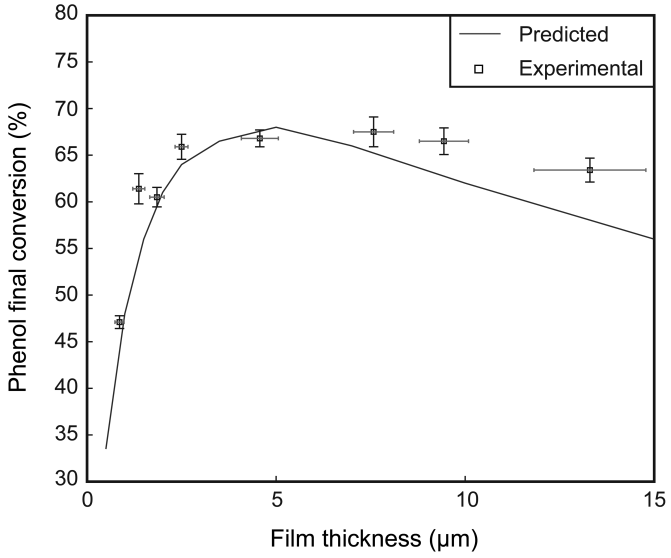

Figure 5: SS configuration. Comparison between predicted and experimental final phenol conversions. Reaction time 3 hours, E_0= 65.3 W m^{-2}. Experimental results are reported with 95% confidence intervals for both average thickness and final phenol conversion values.

and photocatalytic activity are strictly related, is representative of a catalyst in which the transport of species in the solution phase is not significantly limiting the rate of reaction. In addition, in the case of SS illumination (Fig. 5), the model predictions match the experimental results well and show that an optimal film thickness exists at a value of 5 µm.

While the modelling results reported in Fig. 4 and Fig. 5 already provide a good fit to the experimental data, two considerations can be made about the parameters used to solve the governing equations (Table 2). The kinetic parameters used so far have all been experimentally evaluated from previous work and, naturally, have an associated confidence interval. Secondly, the porosity values were obtained from a graphical analysis of a number of FE-SEM images. While the analysis gave the average reported value of 0.57, it is important to notice that a change in the porosity could significantly influence the final results. In fact, the porosity value appears directly in the diffusion terms of the governing equations and in the semi-empirical equation used to calculate the effective diffusion of organic materials in the porous structure (Eq. 9). Moreover, as presented by Ni *et al.*[40],the porosity and morphology of the films will also influence the light absorption characteristics of the film. Analysing available literature Ni and co-authors were able to model, amongst other things, the relationship between the porosity of titanium dioxide films and the consequent change in their light absorption coefficient (i.e. the higher the porosity the lower the light absorption coeff.). Additionally, it must acknowledged that the model presents a simplified picture of the transport within the film. It does not account the possible transport of reactive species like hydroxyl radicals. Their importance in the photocatalytic reaction has

been widely recognised[41, 42, 43, 44] but their ability to diffuse inside and outside the photocatalytic medium is still under investigation. While proof of this phenomenon has been already reported[41, 45], especially for gaseous carriers[46], a reliable and quantitative analysis has not been proposed yet. By running the proposed model with a range of porosity ($\varepsilon_{\mathrm{sol}}$) values between 0.3 and 0.7, the curves presented in Fig. 6 for LS illumination and Fig. 7 for SS illumination were obtained. In this simulations the light absorption coefficient of the hypothetical films were corrected by applying the trend that could be extrapolated from the literature analysis of Ni *et al.*[40]. Assigning a coefficient of 1 to the light absorption coefficient measured for the films used in this work, coefficients of 1.55, 1.34, 1.14, 0.94 and 0.73 were applied to obtain the light absorption coeff. for the range of hypothetical porosities simulated (0.3, 0.4, 0.5,0.6 and 0.7 respectively).

It can be noted that, given the simplifications, the model provides a reliable prediction of the photocatalytic and transport processes inside the material. From Fig. 6 and Fig. 7 it can be noticed how, depending on the illumination configuration, the change in porosity will affect the photocatalytic activity of the film. The change in porosity will affect both the diffusion of the pollutants in Eqns. (5),(6),(7), and (9), where the lower the porosity the lower the diffusivity, and will also influence parameter A in (Eq.10) were the surface of the film is accounted for so that the proper reaction kinetic parameters can be used.

Where LS illumination is employed (Fig. 6), it can be noticed that the change in porosity will have an effect on its actual position, but a plateau will always be reached. Lower porosity, with the consequent higher absorption co-

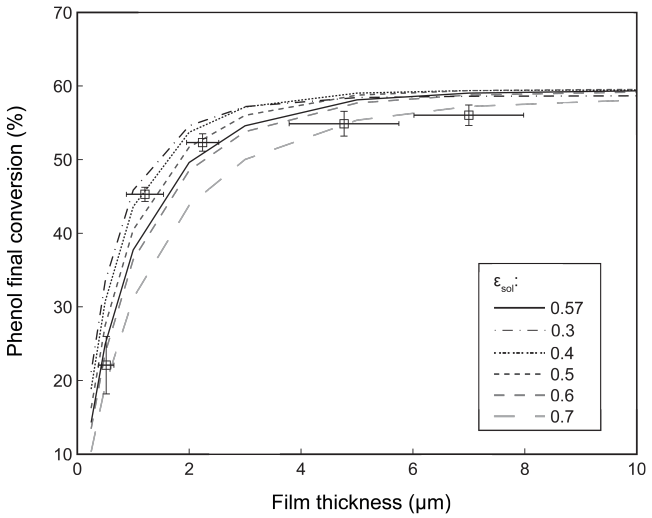

Figure 6: LS configuration. Comparison between predicted final phenol conversions obtained from a range of porosity values. Reaction time 2 hours, E_0= 70.7 W m^{-2}.

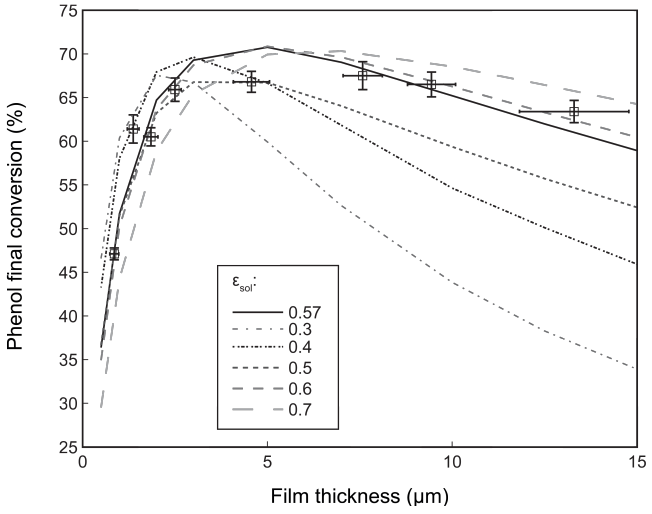

Figure 7: SS configuration. Comparison between predicted final phenol conversions obtained from a range of porosity values. Reaction time 3 hours, E_0= 65.3 W m^{-2}.

efficient, will reach the plateau of maximum conversion at a smaller thickness (3-4 µm); higher porosity and absorption coefficients will delay the plateau to higher thicknesses (8-10 µm). When SS illumination is adopted (Fig. 7), the change in porosity will greatly influence the conversion obtained at increasing thickness values. In this configuration, the extreme cases of very low porosity (ε_{sol}=0.3) will dictate a very strong light absorption and a very slow diffusion of pollutants through the film from the glass/film interface to the liquid/film boundary, moving the optimal catalyst thickness to values close to 1-2 µm and producing a rapid decrease in the obtained photocatalytic degradation if the optimal thickness value is overcome. At increasingly higher porosity values, the optimal thickness value stabilises at approximately 5 µm and, if the thickness is increased over such value ,the decrease in observed pollutant conversion becomes less prominent due to the increased diffusivity of the molecule inside the porous media and the lower absorption coefficient that will facilitate the activation of catalyst layers closer to the solid/liquid boundary (i.e.ε_{sol}=0.7).

Returning to the porosity value obtained from the films used for the study (ε_{sol}=0.57) and including the confidence intervals on the kinetic values obtained from our previous calculation it can be seen from Fig. 8 that the experimental results fall within the confidence interval of the experimentally measured kinetic parameters. This result further confirms the quality of the model adopted the reliability of the porosity evaluation process and the ability of the method proposed in the previous publication[24] to provide intrinsic reaction kinetic parameters.

The ability of the proposed model and the kinetic parameters adopted to

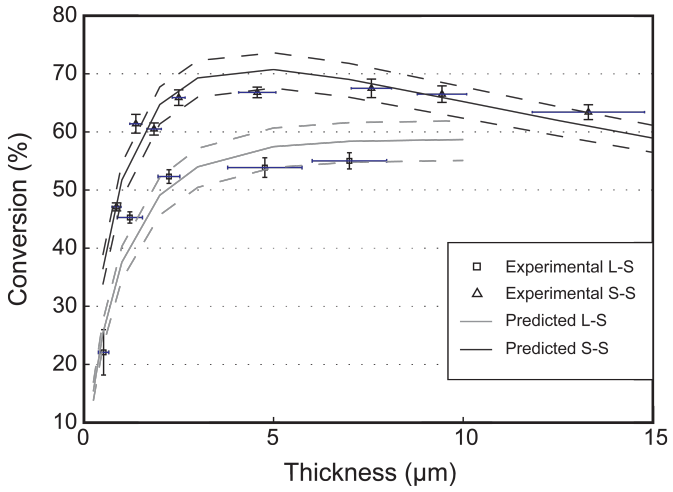

Figure 8: Comparison of SS and LS illumination experimental results with the predicted values. Dotted lines represent the predictions obtained accounting for the kinetic parameters confidence intervals.

describe the photocatalytic reaction is also demonstrated by comparing the predicted bulk concentrations of phenol and intermediates with their analytically measured values. To illustrate this, three of the experimental results obtained with SS illumination using films of 0.86, 4.57 and 13.33 μm average thickness are compared with the analogous model predictions in Fig. 9. A very good correspondence between the model predictions and the experimental results is again observed.

This section is concluded by noting that in this particular application, terms in Eqns. (5) to (8) are small (10^{-10} to 10^{-12} ms^{-1}) in comparison to those for diffusive transport. This is because the net volume change between reactant and products, embodied in the right-hand-side of Eq. (12), which determines the magnitude of the advection in our film, is small. Consequently, the model could be further simplified by neglecting advective transport. However, it was

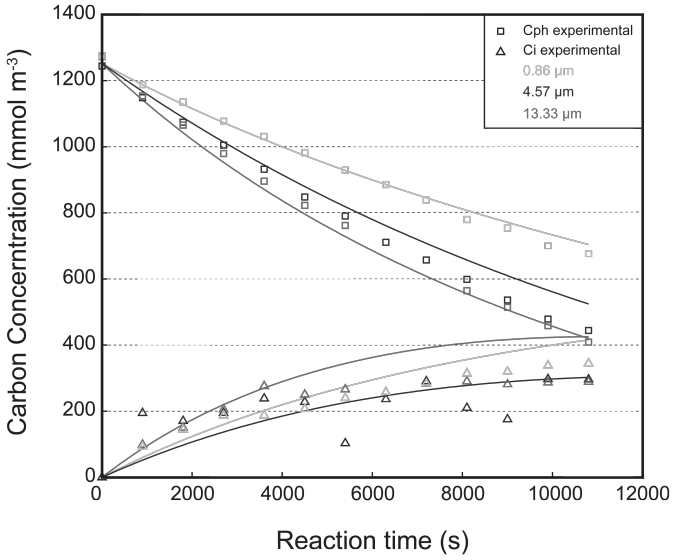

Figure 9: Comparison between predicted and experimental degradation curves(phenol and intermediate products) for 0.86, 4.57 and 13.33 µm films.

chosen not to do so as the model presented is more generally applicable to flow through reacting thin films. Advective terms could become dominant, for example, if in our reactor the porosity of the film is increased and/or the bulk flow is directed at a more perpendicular angle with respect to the plane of the film.

5. Conclusions

In conclusion, this work confirmed experimentally and mathematically that an optimum catalyst film thickness does exist for SS illumination arrangements. The optimum value,for the tested films, is considered to be 5 µm and it is in agreement with that previously estimated by Chen et al.[14] for dip-coated titania films. This parameter can now be used to design and built

efficient photocatalytic reactors that use spray-coated Degussa P25 films. The mathematical model composed by Eqns. (5-7, 12) simply relies on the evaluation of the effects of pollutants diffusion, light absorption and the rate of photocatalytic reaction to predict the pollutants concentration profiles both inside the porous film and in the bulk of the fluid inside a flat plate reactor. Very good agreement between experimental and predicted phenol and TOC conversion was obtained for both LS and SS illumination arrangements. The investigation showed that internal diffusion of light and pollutants can become the limiting factor. It must be stressed that the very good general agreement between model and experimental results was obtained without using any "free" parameter or fitting a large number of variables but, instead, only using coefficients that were experimentally measured or obtained from well-established literature. As long as they are extrapolated in the correct way, like the one proposed in a previous publication [24], intrinsic kinetic parameters previously calculated could be used in the porous film model presented here by using the unitless coef. A of Eq. (10). This means that kinetic data obtained experimentally from films of any thickness can be now employed to solve the model developed in this work and predict how changes in film thickness will effect pollutant conversion in the photocatalytic flat plate reactor. Moreover, as demonstrated here, the model will be able to predict the effects that an eventual change in film porosity obtained by changing material synthesis procedures will have on the effective diffusivity and light absorption coefficient in the film and, as a consequence, on the final pollutant conversion and the optimal thickness value.

6. Acknowledgements

This work was supported by the Australian Research Council (ARC - LP0776793). The authors are also grateful for the funding provided by the Queensland Government under the Smart State Fellowship program. The authors would like to thank the Martens Group, with Mr Ashley Locke, Mr Henry Spratt, Mr Matthew Hales and Mr James Brady, the School of Chemistry , in the persons of Dr Chris Carvalho and Mrs Leonora Newby, and Mr Nathaniel Raupp for the support with the analytical and laboratory work. the Authors would also like to thank Prof. Arne Roos, Uppsala University, for the support in the evaluation of the films light absorption characteristics.

References

[1] G. Centi, S. Perathoner, Catalysis, a driver for sustainability and societal challenges, Catalysis Today 138 (1-2) (2008) 69–76.

[2] P. R. Gogate, A. B. Pandit, A review of imperative technologies for wastewater treatment ii: hybrid methods, Advances in Environmental Research 8 (3-4) (2004) 553–597.

[3] A. Alexiadis, I. Mazzarino, Design guidelines for fixed-bed photocatalytic reactors, Chemical Engineering and Processing 44 (4) (2005) 453–459.

[4] I. D. C. Mazzarino, Feasibility analysis of photocatalytic wastewater treatment, Progress in Water Resources 3 (Water Pollution VI) (2001) 113–122.

[5] A. E. Cassano, C. A. Martin, R. J. Brandi, O. M. Alfano, Photoreactor analysis and design: Fundamentals and applications, Ind. Eng. Chem. Res. 34 (7) (1995) 2155–201.

[6] M. R. Hoffmann, S. T. Martin, W. Choi, D. W. Bahnemann, Environmental applications of semiconductor photocatalysis, Chem. Rev. 95 (1995) 69–96.

[7] M. F. J. Dijkstra, H. J. Panneman, J. G. M. Winkelman, J. J. Kelly, A. A. C. M. Beenackers, Modeling the photocatalytic degradation of formic acid in a reactor with immobilized catalyst, Chemical Engineering Science 57 (22-23) (2002) 4895–4907.

[8] A. E. Cassano, O. M. Alfano, Reaction engineering of suspended solid heterogeneous photocatalytic reactors, Catalalysis Today 58 (2-3) (2000) 167–197.

[9] G. Li Puma, A. Brucato, Dimensionless analysis of slurry photocatalytic reactors using two-flux and six-flux radiation absorption-scattering models, Catalysis Today 122 (1-2) (2007) 78–90.

[10] G. Li Puma, P. L. Yue, Modelling and design of thin-film slurry photocatalytic reactors for water purification, Chemical Engineering Science 58 (11) (2003) 2269–2281.

[11] J. Colina-Marquez, F. Machuca-Martinez, G. L. Puma, Radiation absorption and optimization of solar photocatalytic reactors for environmental applications, Environmental Science and Technology 44 (13) (2010) 5112–5120.

[12] W. Choi, J. Y. Ko, H. Park, J. S. Chung, Investigation on TiO_2-coated optical fibers for gas-phase photocatalytic oxidation of acetone, Applied Catalysis B: Environmental 31 (2001) 209–220.

[13] N. Quici, M. L. Vera, H. Choi, G. L. Puma, D. D. Dionysiou, M. I. Litter, H. Destaillats, Effect of key parameters on the photocatalytic oxidation of toluene at low concentrations in air under 254+185 nm uv irradiation, Applied Catalysis B-Environmental 95 (2010) 312–319.

[14] D. Chen, F. Li, A. K. Ray, External and internal mass transfer effect on photocatalytic degradation, Catalysis Today 66 (2-4) (2001) 475–485.

[15] G. Camera-Roda, F. Santarelli, Optimization of the thickness of a photocatalytic film on the basis of the effectiveness factor, Catalysis Today 129 (1-2) (2007) 161–168.

[16] A. K. Ray, A. A. C. M. Beenackers, Novel swirl-flow reactor for kinetic studies of semiconductor photocatalysis, AIChE Journal 43 (10) (1997) 2571–2578.

[17] V. K. Pareek, A. A. Adesina, Handbook of Photochemistry and Photobiology - Chapter 9: Analysis of photocatalytically reactive systems: kinetic modeling and reactor design via computational fluid dynamics, American Scientific Publisher, 2003.

[18] R. Changrani, G. B. Raupp, Monte carlo simulation of the radiation field in a reticulated foam photocatalytic reactor, AIChE J. 45 (1999) 1085–1094.

[19] G. B. Raupp, J. A. Nico, S. Annangi, R. Changrani, R. Annapragada, Two-flux radiation-field model for an annular packed-bed photocatalytic oxidation reactor, AIChE J. 43 (1997) 792–801.

[20] G. E. Imoberdorf, H. A. Irazoqui, A. E. Cassano, O. M. Alfano, Photocatalytic degradation of tetrachloroethylene in gas phase on TiO_2 films: A kinetic study, Industrial & Engineering Chemistry Research 44 (2005) 6075–6085.

[21] C. R. Esterkin, A. C. Negro, O. M. Alfano, A. E. Cassano, Radiation field inside a reactor of glass-fiber meshes coated with TiO_2, AIChE J. 48 (2002) 832–845.

[22] S. V. Patankar, Numerical Heat Transfer and Fluid Flow, Taylor & Francis, 1980.

[23] H. T. Chang, N.-M. Wu, F. Zhu, A kinetic model for photocatalytic degradation of organic contaminants in a thin-film TiO_2 catalyst, Water Research 34 (2) (2000) 407–416.

[24] M. Vezzoli, W. N. Martens, J. M. Bell, Investigation of phenol degradation: True reaction kinetics on fixed film titanium dioxide photocatalyst, Applied Catalysis A: General 404 (1-2) (2011) 155–163.

[25] M. Montalti, Handbook of photochemistry, 3rd Edition, Taylor and Francis, 2006.

[26] S. L. Murov, G. L. Hug, I. Carmichael, Handbook of photochemistry, M. Dekker, 1993.

[27] W. A. Jacoby, D. M. Blake, R. D. Noble, C. A. Koval, Kinetics of the oxidation of trichloroethylene in air via heterogeneous photocatalysis, Journal of Catalysis 157 (1995) 87–96.

[28] R. B. Bird, W. E. Stewart, E. N. Lightfoot, Transport Phenomena, Wiley, New York, 2006.

[29] K. R. Westerterp, W. P. M. v. Swaaij, A. A. C. M. Beenackers, Chemical reactor design and operation, Chichester : Wiley, 1987.

[30] G. F. Froment, K. B. Bischoff, Chemical reactor analysis and design, New York : Wiley, 1979.

[31] V. F. Stone, R. J. Davis, Synthesis, characterization, and photocatalytic activity of titania and niobia mesoporous molecular sieves, Chemistry of Materials 10 (5) (1998) 1468–1474.

[32] CRC Handbook of Chemistry and Physics, CRC Press, Cleveland, Ohio, 2010.

[33] B. Jahne, G. Heinz, W. Dietrich, Measurement of the diffusion coefficients of sparingly soluble gases in water, J. Geophys. Res. 92 (C10) (1987) 10767–10776.

[34] M. I. Cabrera, O. M. Alfano, A. E. Cassano, Absorption and scattering coefficients of titanium dioxide particulate suspensions in water, Journal of Physical Chemistry 100 (51) (1996) 20043–20050.

[35] P. Atkins, J. dePaula, Physical Chemistry, W. H. Freeman, 2001.

[36] T. K. Sherwood, R. L. Pigford, C. R. Wilke., Mass Transfer, McGraw-Hill, New York, 1975.

[37] MathWorks, Mathematical Functions - Nonlinear Numerical Methods (2011).

[38] V. Hynek, L. Hnedkovsky, I. Cibulka, A new design of a vibrating-tube densimeter and partial molar volumes of phenol(aq) at temperatures from 298 K to 573 K, The Journal of Chemical Thermodynamics 29 (11) (1997) 1237 – 1252.

[39] W. J. Parkinson, N. J. De Nevers, Partial molal volume of carbon dioxide in water solutions, Industrial and Engineering Chemistry Fundamentals 8 (4) (1969) 709–713.

[40] M. Ni, M. K. Leung, D. Y. Leung, K. Sumathy, An analytical study of the porosity effect on dye-sensitized solar cell performance, Solar energy Materials & Solar Cells 90 (2006) 1331–1344.

[41] C. S. Turchi, D. F. Ollis, Photocatalytic degradation of organic water contaminants: mechanisms involving hydroxyl radical attack, Journal of Catalysis 122 (1) (1990) 178–92.

[42] O. M. Alfano, M. I. Cabrera, A. E. Cassano, Photocatalytic reactions involving hydroxyl radical attack, Journal of Catalysis 172 (2) (1997) 370–379.

[43] S. Brosillon, L. Lhomme, C. Vallet, A. Bouzaza, D. Wolbert, Gas phase photocatalysis and liquid phase photocatalysis: Interdependence and

influence of substrate concentration and photon flow on degradation reaction kinetics, Applied Catalysis B: Environmental 78 (3-4) (2008) 232–241.

[44] E. R. Carraway, A. J. Hoffman, M. R. D. C. Hoffmann, Photocatalytic oxidation of organic acids on quantum-sized semiconductor colloids, Environmental Science and Technology 28 (5) (1994) 786–93.

[45] S. Kim, W. Choi, Kinetics and mechanisms of photocatalytic degradation of $(CH_3)_nNH_4^+$ in TiO_2 suspension: The role of OH radicals, Environ. Sci. Technol. 36 (9) (2002) 2019–2025.

[46] Y. Murakami, E. Kenji, A. Y. Nosaka, Y. Nosaka, Direct detection of oh dadicals diffused to the gas phase from the uv-irradiated photocatalytic TiO_2 surfaces by means of laser-induced fluorescence spectroscopy, J. Phys. Chem. B 110 (34) (2006) 16808–16811.